GABOR TRANSFORM FOR SUBBAND SAS IMAGING

J. Wilbur, R. J. McDonald and D. Brown
Code HS, NSWCPC West Hwy 98
Panama City Beach, FL 32407
joellen.wilbur@navy.mil

Abstract - **This paper describes a method for integrating a frequency-dependent object characterization into a practical sonar imaging system. Integration of joint time-frequency (JTF) processing into broadband SAS imaging enables one to add another dimension (frequency) to the object feature space without compromising resolution. JTF processing enables a user to construct a 3-D image description around objects of interest. The Gabor transform is used to capture the local frequency behavior in the image. The Gabor coefficients are used to reconstruct multispectral images.**

I. INTRODUCTION

Broadband sonars provide an added dimension of information and with that the opportunity to selectively retain important object information while eliminating geological features not associated with the object. Success relies on effective processing and interpretation of the frequency information. Physics based object models of acoustic backscatter use frequency as a prime variable, often defined in terms of radius, a, and acoustic wavenumber, k. For example, fluid filled spheres insonified at low frequencies exhibit sharp peaks and nulls in the acoustic backscatter. [1] As ka increases marine biologists have predicted and observed a frequency variation in object strength associated with shape in the acoustic return of biologics that conform to fluid filled and elastic object models. [2]

The object response to an incident broadband waveform is the superposition of an aspect dependent specular response and an aspect independent free oscillation period [1-4]. The early-time response is referred to as the specular response from the surface as the incident pulse traverses the object. The late-time response, or free oscillation period, is due to energy deposited into the object and contains the natural frequencies of the object [1-4]. Each natural frequency of the object has a characteristic beampattern associated with it and the collection of frequency bands represents the object response. Object characterization relies on information from both the broadband frequency independent scattering centers of the object and frequency dependent information that arises from localized and dispersive mechanisms associated with object structure [1-4].

Application of time-frequency concepts to study the acoustic response from elastic objects has been well documented [1,2,5,6,7]. Several papers have explored the potential merits of an expanded object description and purported time-frequency concepts to offer a robust feature set for object classification. Sessarego, Sageloli, Flandrin, and Zakharia [1], among others, have used various forms of the Wigner representation for a time-frequency characterization of the acoustical scattering from a spherical shell. In their analysis they observed velocity dispersion of certain surface waves. Subsequent time-scale analyses of the scattering from spherical shells have produced similar observations. Pinto, Belletini, Hollett and Tesei [7] observed the echo response from a partially buried spherical shell in the spectrogram of the maximum object response of beamformed data.

In this paper we merge a form of JTF processing applied to radar images by Chen and Ling [4] with a SAS wavenumber imaging algorithm to develop a frequency dependent sonar image description (range, cross-range, frequency) for object characterization.

Our processor is designed to first create a broadband image over a large viewing area. When the sonar enters an investigation mode, the user defines a rectangular region of interest by moving the mouse over the image and clicking to define a boxed area for examination and feature extraction. This process can alternatively be automated. Figure 1 below illustrates the broadband image output and region of selection for creating the *(x,y,f)* volume image.

Report Documentation Page

1. REPORT DATE	2. REPORT TYPE	3. DATES COVERED
01 SEP 2006	**N/A**	**-**

4. TITLE AND SUBTITLE	5a. CONTRACT NUMBER
Gabor Transform For Subband Sas Imaging	5b. GRANT NUMBER
	5c. PROGRAM ELEMENT NUMBER

6. AUTHOR(S)	5d. PROJECT NUMBER
	5e. TASK NUMBER
	5f. WORK UNIT NUMBER

7. PERFORMING ORGANIZATION NAME(S) AND ADDRESS(ES)	8. PERFORMING ORGANIZATION REPORT NUMBER
Code HS, NSWCPC West Hwy 98 Panama City Beach, FL 32407	

9. SPONSORING/MONITORING AGENCY NAME(S) AND ADDRESS(ES)	10. SPONSOR/MONITOR'S ACRONYM(S)
	11. SPONSOR/MONITOR'S REPORT NUMBER(S)

12. DISTRIBUTION/AVAILABILITY STATEMENT
Approved for public release, distribution unlimited

13. SUPPLEMENTARY NOTES
See also ADM002006. Proceedings of the MTS/IEEE OCEANS 2006 Boston Conference and Exhibition Held in Boston, Massachusetts on September 15-21, 2006, The original document contains color images.

14. ABSTRACT

15. SUBJECT TERMS

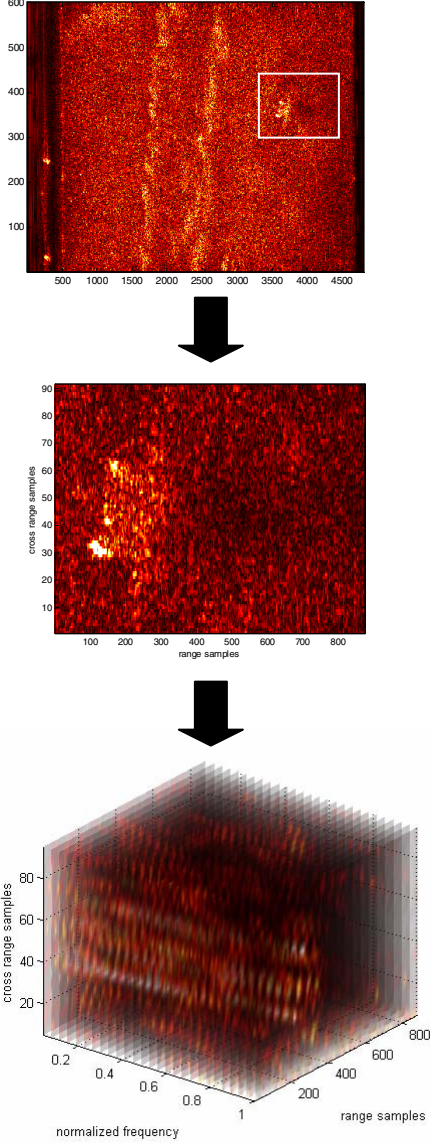| 16. SECURITY CLASSIFICATION OF:			17. LIMITATION OF ABSTRACT	18. NUMBER OF PAGES	19a. NAME OF RESPONSIBLE PERSON
a. REPORT	b. ABSTRACT	c. THIS PAGE	**UU**	**5**	
unclassified	**unclassified**	**unclassified**			

Figure 1. Volume processing for *(x,y,f)* image representation of selected region.

Volume characterization is valuable to the interpretation of the data, especially from buried objects where geometric and shadow information is incomplete or unavailable. The following section describes the processing for *(x,y,f)* image formation.

II. *V(X,Y,F)* IMAGE FORMATION

The excitation signal is a linear chirp, *c(t),* designed to sweep across the frequency band of interest. The waveform samples *d(m,n),* along mT_s, for each ping *n,* are related to the object reflectivity density, $p(x,y)$, through a sampled convolution of the form

$$d(m,n) = \int_{-\infty}^{\infty} (\hat{s}_n(t) \underset{t}{*} c(t))\delta(t - \frac{m}{f_s})dt \qquad (1)$$

where

$$s_n(t) = \iint_{x\ y} p(x,y)\delta(t - \frac{1}{c}r_n(x,y))dxdy \qquad (2)$$

$$r_n(x,y) = \sqrt{x^2 + (y - n\Delta_u)^2}$$

for $\hat{s}_n(t) = s_n(t) + b(t)$ and *b(t)* is bottom scattering and $s_n(t)$ is the impulse response function of the object at the *nth* ping.   Inverse filtering of the data yields $\hat{s}_n(t) \rightarrow s_n(t)$. [7,8]

For **d** the MxN sampled data matrix in (1) and H_m, *m=1,2,...,M* the FIR filter coefficients of the inverse filter where

$$\mathbf{H} = \begin{bmatrix} H_1 & & & \\ & H_2 & & 0 \\ & & \ddots & \\ & & & \ddots \\ 0 & & & \\ & & & H_M \end{bmatrix} \qquad (3)$$

and **U** and **Q** are respective DFT matrices of order MxM and NxN then the data transfer function matrix is calculated as

$$\mathbf{S = HQdU}^T \qquad (4)$$

where $Q_{lm} = W_M^{-lm}$ and $U_{kn} = W_N^{-kn}$ for $W_L \equiv e^{j\frac{2\pi}{L}}$.

The matrix in (4) is defined as the object transfer function in frequency and Doppler wavenumber, $S(\omega, k_u)$, and is related to (2) through 2-D Fourier transform.

The type 2 wavenumber algorithm [8,10,11] is used to form the image. The wavenumber algorithm derives from the principle of stationary phase where the relationship below forms the premise behind the algorithm

$$S(\omega, k_u) \propto \iint p(x,y)e^{-j\left(\sqrt{(\frac{2\omega}{c})^2 - k_u^2} + k_u^2\right)}dxdy . \qquad (5)$$

Coordinate warping of the axis from $\omega \rightarrow \frac{c}{2}\sqrt{k_x^2 + k_u^2}$, $k_y = k_u$ is used to map (4) into the transform $P(k_x,k_y)$ where k_x and k_y are the spatial Doppler frequency variables in the along track and cross-track

directions. This enables a 2-D Fourier transform operation directly on $P(k_x,k_y)$ to form the image.

Using the relation in (5), the reflectivity density function, $p(x,y)$, is calculated from (4) as follows

$$\mathbf{p} = \frac{1}{M}\mathbf{Q}^H \mathbf{E}\hat{\mathbf{P}}\mathbf{U}^{-1} ; \qquad (6)$$

where

$$\hat{\mathbf{P}} = \left[\mathcal{S}\{\mathbf{A}\}\right]; \quad \mathcal{S} \equiv \text{Stolt interpolation}$$

for

$$A_{lk} = S_{lk}T_{lk} ; \quad T_{lk} = e^{-j\frac{M-1}{2}\sqrt{\frac{4}{c^2}\left(\frac{2\pi l}{M}\right)^2 - \left(\frac{k}{N}\right)^2}} ,$$

and $\mathbf{E}$ is a diagonal matrix with nonzero elements $e^{-j\frac{M-1}{2}\frac{l'}{M}}$, $l' = 0,1,2,...,M-1$.

The image mapping in (6) can be interpreted as a mapping of the object reflectivity function. For simple scattering image peaks correspond spatially along the horizontal range direction to the scattering centers on the object. Objects with complex scattering also exhibit image artifacts from localized components associated with the natural frequencies of the object[4].

The natural frequencies of the object associated with the free oscillation period are distinguished by a Gabor transform at each cross range position[4,12]. The Gabor expansion in the horizontal range direction is

$$p(n,m) = \sum_{m',k} \left\langle p_n, g_{m',k}\right\rangle h_{m',k}(m) \qquad (7)$$

where

$$\sum_{m',k} g^*_{m',k}(i)h_{m',k}(j) = \delta(i-j) \qquad (8)$$

The inner products $\left\langle p_n, g_{m',k}\right\rangle$ form the Gabor coefficients and can be calculated using an FFT as

$$V_{nm'k} = \sum_m p_n(m)g(m-m'\Delta M)W_K^{-mk} \qquad (9)$$

where K is the number of frequency channels and ΔM is range interval between samples. The coefficients in (9) describe at each n the local JTF behavior around $(m'\Delta M,k)$.

The Gabor coefficients were used to plot the volume image in Figure 1. The frequency behavior can be seen looking down from the top into the x-f plane of the volume as in Figure 2a. Here a broadband specular scatterer dominates the volume image followed by some

localized bands. Figure 2b is the volume rotated to view into the x-y image plane.
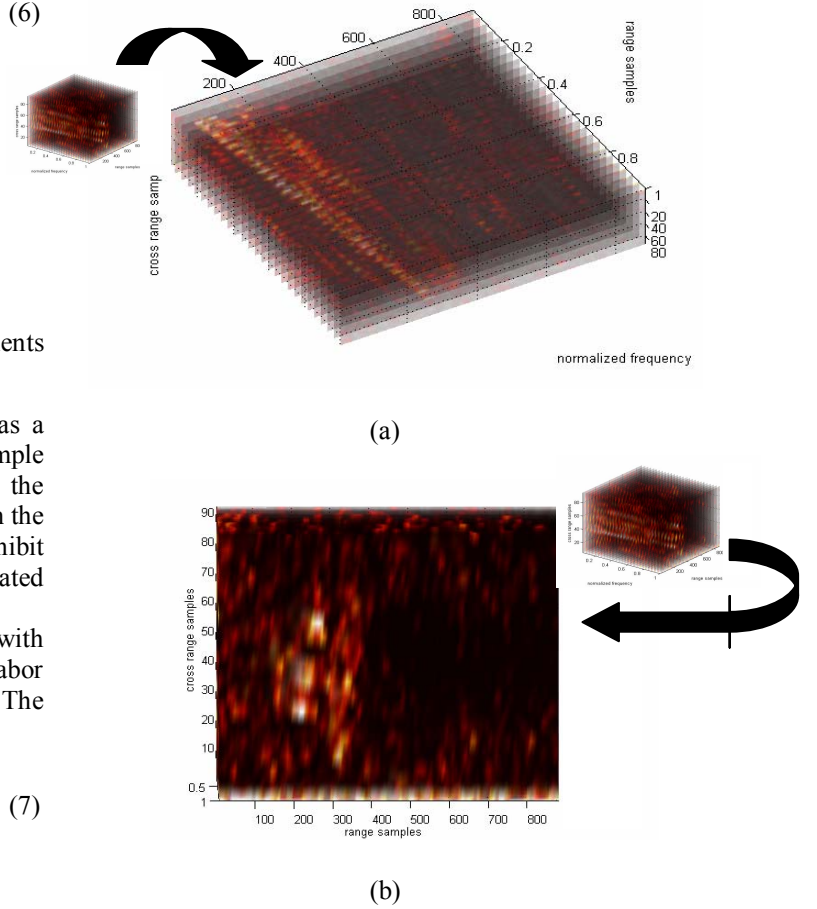

(a)

(b)

Figure 2. Volume image from the target (a) viewed into the x-f plane (b) viewed into the x-y image plane.

III. SUB-BAND IMAGE RECONSTRUCTION

In creating the volume image $K > \Delta M$ where coefficient sampling is high and $g(m)$ approximates the normalized Gaussian. For this case $h(k) \approx cg(k)$ [12]. This enables reconstruction of the image from (7) and (8) making sub-band image reconstruction possible. This becomes clear by expressing the Gabor coefficients in (9) as a vector of K narrowband frequency images of the form

$$\mathbf{V}(n,m') = \left[V_0(m',n) \quad V_1(m',n) \quad ... \quad V_{K-1}(m',n)\right]^T \qquad (10)$$

From (10) each pixel position (n,m') is described by a frequency vector of length K. Representation of the

volume is effectively a series of narrowband image planes at each frequency center $k=0,1,...K-1$. Sub-band image reconstruction from the Gabor coefficients enables a flexible process for narrowband characterization of the *x-y* image. Figure 3 illustrates the process.
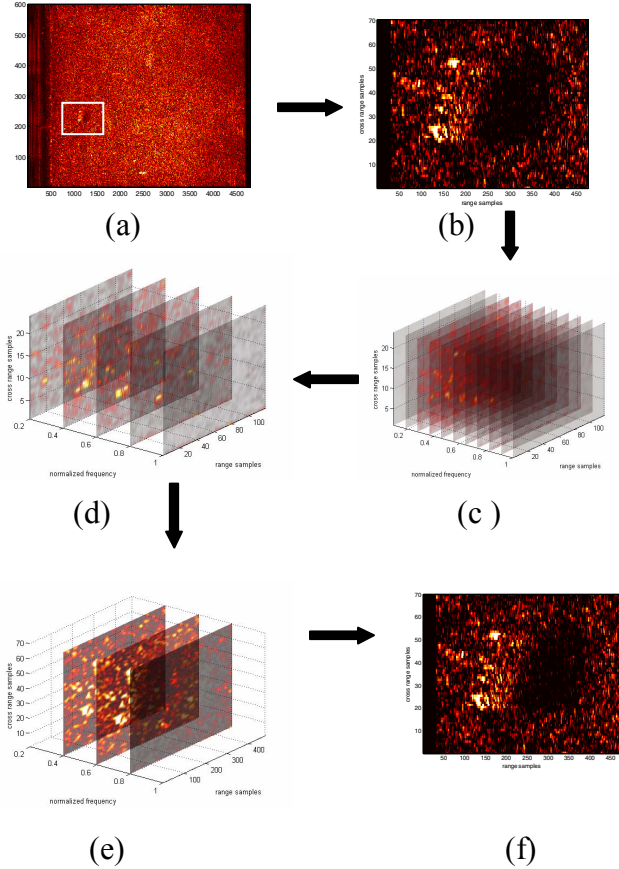

(a)

(b)

(d)

(c)

(e)

(f)

Figure 3. Varying levels of narrowband image reconstruction from Gabor coefficients. (a) Large broadband swath. (b) Broadband image of selected object. (c) Narrowband slice planes from Gabor transform. (d) Image reconstruction into 5 frequency sub-bands. (e) Image reconstruction into 3 sub-bands. (f) Image reconstruction over entire band.

IV. CONCLUDING REMARKS

We introduce a frequency based imager (range, cross-range, frequency) for object characterization using broadband active sonar. The imager is designed to discriminate scattering centers or the short period broadband portions of the object backscattered return from localized portions attributable to natural frequencies and mechanical structure. In essence, each *(x,y)* image pixel is described by a vector of frequencies with magnitude and phase. The *(x,y,f)* image is constructed from the Gabor coefficients and enables flexible sub-band reconstruction of the object.

The object strength in any frequency band may be calculated from their respective Gabor coefficients. The processor can be interpreted as an adaptive imager with an automatic discrimination between localized and broadband events. Further research includes weighting of the Gabor coefficients prior to image reconstruction to form a composite image that accentuates localized object features normally dominated by the broadband portions in the original image.

REFERENCES

[1] J.P. Sessarago, J. Segaloli, P. Flandrin, and M. Zakharia, "Time-Frequency Analysis of Signals Related to Scattering Problems in Acoustics. Part I: Wigner-Ville Analysis of Echoes Scattered by a Spherical Shell," in *Wavelets: Time Frequency Methods and Phase Space*, ed. J.M. Combes, A. Grossmann, and Ph. Tchamitchian, (Springer-Verlag, NY, 1988), pp.147-153.

[2] J. Wilbur and N.P. Baum, "Acoustic Singularity Identification," in *Detection and Identification of Visually Obscured Targets*, ed. C.E. Baum, (Taylor and Francis, Washington DC, 1996), Chap. 10.

[3] J. McCorkle, V. Sabio, R. Kapoor, and N. Nandhakumar, "Transient Synthetic Aperture Radar and the Extraction of Anisotropic and Natural Frequency Information," in *Detection and Identification of Visually Obscured Targets*, ed. C.E. Baum, (Taylor and Francis, Washington DC, 1996), Chap. 12.

[4] V.C. Chen and H. Lang, "Joint Time-Frequency Analysis for Radar Signal and Image Processing," *IEEE Signal Processing*, Vol. 16 No. 2, March 1999.

[5] C. Baudet, O. Michel, and W. Williams, "Detection of coherent structures using time-scale resolved acoustic spectroscopy," arXiv:chao-dyn/9804010 v2, Nov. 1998.

[6] M. Till and S. Rudolph, "Optimized time-frequency distribution for acoustic signal classification," *Proc. SPIE*, VIII, Orlando, FL, April 2001.

[7] M.A. Pinto, A. Bellettini, R. Hollet and A. Tesei; "Real and Synthetic-Array Signal Processing of Buried Targets" *IEEE Journal of Oceanic Engineering* Vol. 27 No. 3, July 2002, pp. 484-494.

[8] R. Bamler, "A Comparison of Range-Doppler and Wavenumber Domain SAR Focusing Allgorithms," *IEEE Transactions on Geoscience and Remote Sensing*, Vol. 30 No. 4, July 1992.

[9] J.R. Sacha and B.L. Johnson, "A constrained iterative multiple operator deconvolution technique," *J. Acoust. Soc. Am.,* Vol.96 No. 1, July 1994.

[10] P.T. Gough and D.W. Hawkins, "Imaging Algorithms for Strip-Map Synthetic Aperture Sonar: Minimizing the Effects of Aperture Errors and Aperture Undersampling," *IEEE Journal of Oceanic Engineering* Vol. 22 No. 1, January 1997.

[11] G. Sammelmann, J. Fernandez, J. Christoff, L. Vaizer, J. Lathrop, R. Sheriff, and T. Montgomery, "High frequency/low frequency synthetic aperture sonar," *Proc. SPIE*, vol. 3079, pp. 160-171, 1997.

[12] S. Qian and D. Chen, "Joint Time-Frequency Analysis," *IEEE Signal Processing*, Vol. 16 No. 2, March 1999.